ELSEVIER

Materials Characterization 58 (2007) 997–1005

MATERIALS CHARACTERIZATION

Surface roughness characterization of thermally sprayed and precision machined WC–Co and Alloy-625 coatings

Z.W. Zhong *, Z.F. Peng, N. Liu

School of Mechanical and Aerospace Engineering, Nanyang Technological University, 50 Nanyang Avenue, Singapore 639798, Republic of Singapore

Received 8 December 2005; received in revised form 5 March 2007; accepted 15 May 2007

Abstract

Surface roughness characterization of thermally sprayed and precision machined WC–Co and Alloy-625 coatings was carried out. The objectives were to demonstrate that such difficult-to-machine coating surfaces could be machined with commercial machines and tools, and to characterize the surface finish of the machined coatings. The coatings were obtained using two thermal spraying processes: arc spraying and high velocity oxy-fuel spraying. Different machining techniques were tried to optimize the surface finishing of the coatings based on surface finish and time required. Machined samples were then examined using stylus roughness testers. Surface roughness parameters R_a and R_q were measured using various cut-off lengths, sampling lengths, and numbers of sampling and cut-off lengths to characterize the scaling behavior of the surfaces. Diamond turning of WC–Co demonstrated the advantage of high material removal rates, and diamond grinding of WC–Co produced good surface finish with relatively high material removal rates. Precision-machined WC–Co and Alloy-625 surfaces could be identified as self-affine fractals in a statistical sense within the correlation length, i.e. within the length scales studied from 0.08 to 8 mm. The surface roughness heights of the machined surfaces were found to be dependent on the scale of cut-off length as a power law.

Keywords: WC–Co; Alloy 625; Surface roughness; Cut-off length; Fractal; Grinding; Turning

1. Introduction

WC composites have very high hardness and wear-resistance. The superior wear resistance of WC–Co cermet is determined by evenly distributed fine WC particles bonded to the Co matrix. Increasing the percentage of Co increases the toughness but lowers the hardness and wear-resistance [1–3].

Wear resistant coatings applied on industrial machinery components can reduce weight, increase adhesion strength, decrease internal stresses and improve the resistance against propagation of surface defects [4,5]. Electroplated chromium coatings were accepted for wear-resistant applications because of hardness, low coefficient of friction and corrosion resistance [1]. However, thermally sprayed coatings excel because they do not require toxic chemical baths and can have a greater thickness.

With the rapid development of the high velocity oxy-fuel (HVOF) processes, the application area of WC–Co coatings is expanding successfully and rapidly [6].

* Corresponding author. Tel.: +65 6790 5588; fax: +65 6791 1859.
E-mail address: mzwzhong@ntu.edu.sg (Z.W. Zhong).

1044-5803/$ - see front matter © 2007 Elsevier Inc. All rights reserved.
doi:10.1016/j.matchar.2007.05.010

WC–Co cermets are widely used by thermal spray processes to deposit protective coatings on engineering surfaces against conditions where abrasion, erosion and other forms of wear exist. HVOF processes have been very successful in spraying wear resistant WC–Co coatings with higher density, superior bond strengths and less decarburization than many other thermal spray processes [7]. The wear performance of the WC–Co coatings sprayed by the HVOF process is better than that of the coatings sprayed by plasma, and even comparable with that of detonation gun coatings [8,9].

Nickel-based super-alloys are the most frequently used heat-resisting materials for gas turbines, aircraft engine components, jet engine critical parts, rocket engines, nuclear components, tools and dies for hot working of metals. They are also difficult-to-cut materials [9,10]. Alloys 625 and 718 have been among the most successfully applied nickel-based super-alloys in engineering applications [11].

Because of its many outstanding properties, Alloy 625 is used in the aerospace, nuclear, chemistry, pulp and paper, offshore, onshore and marine industries, and in geothermal power systems [12–16]. Alloy 625 is also used extensively in ship machinery system construction [17].

However, thermally sprayed WC–Co and Alloy 625 coatings on engineering components have very rough surfaces. To transform a raw coating material into a precision engineering component having the desired shape, size and surface quality, it has to be processed by some means. There are different processes in which this transformation can be achieved. Some components are produced by one process, and others are by several processes [18].

WC and WC–Co alloys are usually classified as hard tool materials [19–21] and can be used to machine Alloy 625. To machine such hard tool materials, electrolytic grinding, electrochemical machining, and electrical discharge machining have been conducted [22]. In this study, diamond and CBN (cubic boron nitride) tools were used to machine hard WC–Co coatings and WC–Co tools were used to machine Alloy 625 coatings in order to improve the surface roughness of the coatings.

Apart from the effect of lubrication and hardness, surface roughness is one of the major factors that influence wear rates [1,2]. A quantitative scanning tunneling microscopy study on Ni/Cu(001) has found that surface roughness affects magnetic anisotropy with respect to flat nickel films [23]. Fiber surface roughness is a key parameter affecting the behavior at the fiber-matrix interface and the overall behavior of a composite. Even small changes of fiber roughness can significantly affect the debonding and sliding properties [24].

The roughness of an engineering surface is determined by the finishing process. For example, single-crystal-diamond turning [25] of suitable materials can produce super-smooth mirrors [26]. Diamond grinding can also generate mirror surfaces on brittle materials [27–29]. Mirror-surface finish of hard and brittle materials can be achieved by ductile-mode grinding [30,31].

Surface characterization of machined engineering components plays an important role in modern industry. The knowledge gained about a surface is used to control the surface production process and to predict the performance of the component in its functional environment [32–35]. Surface texture can be measured in many ways. The most common method involves mechanically drawing a stylus across a surface [36]. An atomic force microscope (AFM) measures tip-surface interactions due to forces such as Van Der Waals, electrostatic, frictional and magnetic forces [37]. Basically, an AFM is similar to a stylus instrument, because both are contact measurement devices with a very sharp tip [38]. Besides surface characterization [26], AFMs can also be used to form scanning moiré fringes for inspection of surface deformations [39].

In this study, precision machining and surface roughness characterization of thermally sprayed WC–Co and Alloy-625 coatings were carried out. The objectives were to demonstrate that such difficult-to-machine coatings could be machined with commercial machines and tools, and to characterize the surface finish of the machined coatings. Different machining techniques were compared for optimization of the surface finish with regard to time required and quality of the finish. Machined samples were then examined using stylus roughness testers. Surface roughness parameters R_a and R_q were measured using various cut-off lengths, sampling lengths, and numbers of sampling and cut-off lengths to characterize the scaling behavior of the surfaces.

Table 1
Specimens and tools used for machining of the coatings

Specimens	WC–Co or Alloy 625 coating on steel rod: diameter 63.5 mm, length 120 mm.
Diamond rough-grinding wheel	Resin bond, diameter 305 mm, width 25 mm, mesh No. #200 (200-grit).
Diamond fine-grinding wheel	Resin bond, diameter 305 mm, width 25 mm, mesh No. #1200 (1200-grit).
CBN rough-grinding wheel	Resin bond, diameter 305 mm, width 25 mm, mesh No. #200 (200-grit).
CBN fine-grinding wheel	Resin bond, diameter 305 mm, width 25 mm, mesh No. #1200 (1200-grit).
Turning tools	PCD tools for turning WC–Co. WC–Co tools for turning Alloy 625.

2. Experiments

Table 1 shows the specimens, the turning tools and the grinding wheels used. The coatings on stainless steel or mild steel rods were obtained using two thermal spraying processes: arc spraying and HVOF spraying. The processes evaluated for machining WC–Co coatings were diamond grinding, CBN (cubic boron nitride) grinding, diamond turning and diamond polishing. Emphasis was placed on reducing the machining time for an acceptable surface finish. The process for machining Alloy 625 coatings was turning, using WC–Co tools.

Turning of WC–Co coatings applied by HVOF spraying was performed on a standard lathe using polycrystalline diamond (PCD) tools. Depths of cut used were 0.2 and 0.35 mm. Feed rates were 0.071 and 0.16 mm/rev. The cutting speed range was from 10 m/min to 20 m/min.

Table 2
Coating materials of the four samples and details of the machining processes

Sample ID	HVOF sprayed coating	Substrate	Machining process	Machining conditions
Alloy-1	Alloy 625	Steel rod	Turning using WC–Co	Cutting tool: WC–Co (ISO K20); cutting speed 80 m/minute (400 rpm); feed rate 0.1 mm/rev; depth of cut=0.2 mm.
Alloy-2	Alloy 625	Steel rod	Turning using TiAlN PVD coated WC–Co	Cutting tool: TiAlN PVD coated WC–Co (ISO M15) having micro grains; cutting speed 80 m/min (400 rpm); feed rate 0.1 mm/rev; depth of cut=0.2 mm.
WC–Co-1	WC–Co	Steel rod	Diamond grinding	Diamond grinding wheel: resin bond, diameter 305 mm, width 25 mm, mesh No. #1200 (1200-grit); wheel speed 1440 m/min (1500 rpm); work speed 19 m/min (95 rpm); depth of cut 3 μm; feed speed 200 mm/min.
WC–Co-2	WC–Co	Steel rod	Diamond turning	Cutting tool: polycrystalline diamond; cutting speed 16 m/min (80 rpm); feed rate 0.16 mm/rev; depth of cut 0.2 mm.

Table 3
Surface roughness (R_a) values and material removal rates or machining time of the machining processes evaluated

Process	Material removal rate (mm^3/s)	R_a (μm)
Diamond polishing of WC–Co	(3–3.5 h to remove rough surface, 100 minutes for finishing, total machining time: about 5 h)	0.020–0.026
Diamond/CBN fine grinding of WC–Co	0.667–2.00	0.017–0.1
Diamond/CBN rough grinding of WC–Co	1.25–6.65	0.06–0.62
Diamond turning of WC–Co	2.37–18.7	0.63–1.19
Fine turning of Alloy 625	13.3–53.3	0.14–0.88

Grinding experiments were conducted on a standard cylindrical grinding machine. Rough grinding conditions were depths of cut: 5 and 10 μm, feed rates: 75 and 200 mm/min, wheel speed: 1500 rpm (1440 m/min), and work speeds: 50 rpm (10 m/min) and 95 rpm (19 m/min). Fine grinding conditions were depths of cut: 1 and 3 μm, feed rate: 200 mm/min, wheel speed: 1500 rpm (1440 m/min), and work speed 95 rpm (19 m/min) and 120 rpm (24 m/min).

Only CBN grinding wheels were used for grinding WC–Co coatings obtained by arc spaying, and diamond grinding was not conducted, because WC–Co coatings obtained by arc spraying had a steel matrix and diamond is not suitable for grinding steel.

Turning of Alloy 625 coatings applied by HVOF and arc spraying was conducted on the standard lathe using various WC–Co tools. Depth of cut used was 0.2 mm. Feed rates were 0.1 and 0.2 mm/rev. The cutting speed range was from 40 m/min to 80 m/min.

The surface finish of all the coated rods after machining was measured using contact stylus-type profilometers. The stylus tip radius was 2 μm. The Gaussian filter was selected to measure surface roughness. During measurement, the stylus tip scanning direction was perpendicular to the grinding/turning direction. A V-shaped block facilitated the alignment required for the measurement of the cylindrical surfaces. The machined surfaces were also observed under optical microscopes.

Four HVOF sprayed and precision machined samples were selected and their surface roughness parameters R_a and R_q were measured using various cut-off lengths, sampling lengths, and numbers of sampling and

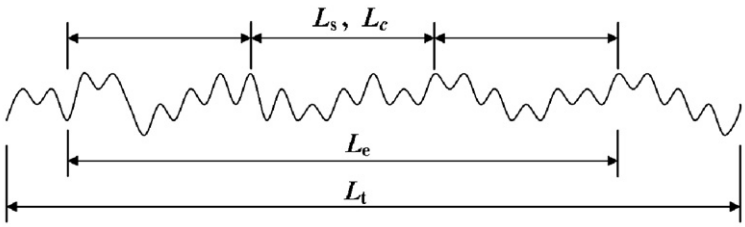

Fig. 1. Various lengths used to characterize a surface profile (L_t = traverse length, L_e = evaluation length, L_s = sampling length, and L_c = cut-off length).

cut-off lengths to characterize the scaling behavior of the surfaces. The materials of the four samples and details of the machining processes are shown in Table 2.

3. Results and discussion

3.1. Machining of the coatings

The material removal rates (MRRs) and the surface roughness (R_a) values of the various machining processes evaluated are listed in Table 3. WC–Co coatings could be turned using polycrystalline diamond (PCD) tools. The turning time needed was much shorter than the grinding time and polishing time to remove the same material volume, because the diamond turning had the highest MRR among all the processes evaluated for machining the WC–Co coatings. However, for all parameters tested, the finished surfaces by the diamond turning were rough with some damaged areas. Also, the diamond inserts tended to chip during turning.

CBN grains tended to be flattened quickly during CBN grinding of the WC–Co alloys. During the CBN grinding of WC–Co coatings sprayed by the HVOF process, there were problems with loading of the rough and fine CBN grinding wheels. This required more dressing operations on the grinding wheels and therefore the total grinding operation time was effectively increased. Some HVOF applied WC–Co samples ground with the CBN fine-grinding wheel showed cracks. However, the hard coatings could be clearly ground by using the CBN fine-grinding wheel when careful dressing operations were conducted often. For the WC–Co (+Fe) coating applied by arc spraying, there was no loading with the CBN wheels. Possible reasons for the lack of loading could be the higher porosity of the arc sprayed coating and the matrix with steel and lower carbide content.

Typical Vickers hardness values of CBN and diamond are 40–50 GPa and 60–70 GPa, respectively [40]. The Vickers hardness values of the WC–Co and Alloy 625 are 0.52 GPa (WC–Co applied by arc spraying), 1.07 GPa (HVOF applied WC–Co), 0.37 GPa (Alloy 625 applied by arc spraying), 0.46 GPa (HVOF applied Alloy 625), respectively [41]. The loading and cracking problem did not occur when diamond grinding was performed, because diamond is much harder than WC–Co alloys.

Mirror-like surfaces were obtained by polishing, or fine grinding using the fine diamond wheel for WC–Co coatings sprayed by the HVOF process and using the fine CBN wheel for WC–Co (+Fe) coatings applied by arc spraying. However, the fine grinding time required

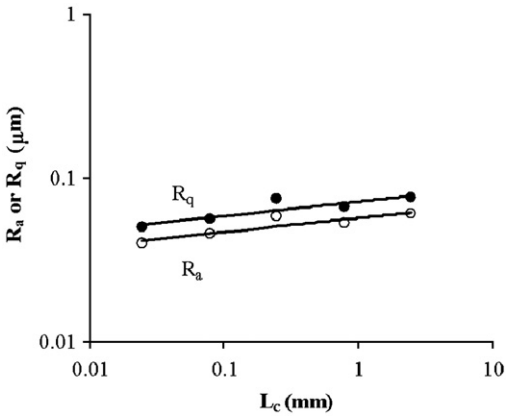

Fig. 2. Surface roughness R_a and R_q versus cut-off length L_c (sample WC–Co-1).

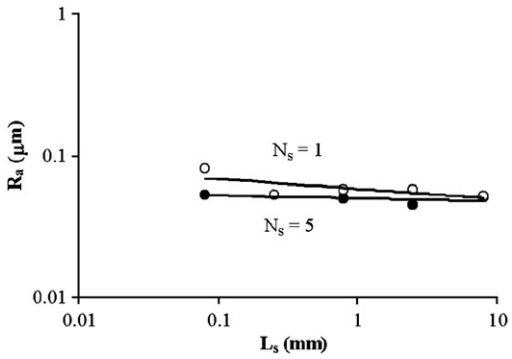

Fig. 3. Surface roughness R_a versus sampling length L_s with N_s = 1 and 5 (sample WC–Co-1).

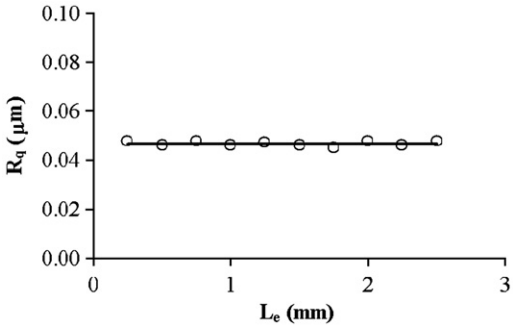

Fig. 4. Surface roughness R_q versus evaluation length L_e (sample WC–Co-1).

to get a mirror-like surface was much shorter than the polishing time required. The total polishing time for rough polishing, honing, pre-final-finishing and final finishing was very long (over 5 h). To reduce the total machining time and cost, rough machining should be conducted by rough grinding or diamond turning, and the final finishing can be fine grinding.

WC–Co tools were hard enough to turn tough Alloy 625 coatings effectively. Compared to those for the Alloy 625 coatings applied by arc spraying, the coatings applied by HVOF spraying were denser and harder, and therefore lower cutting speeds had to be used, but the surface finish was much better.

3.2. Surface roughness characterization

Two widely used surface roughness parameters are R_a, the centerline average or arithmetical average deviation, and R_q, the root-mean-square (RMS) deviation, relative to a mean line (centerline). If $f(x)$ is a profile characterized from the mean line and L is the length, which could be the sampling length, of the profile, R_a and R_q are defined as [18]:

$$R_a = \frac{1}{L}\int_0^L |f(x)|\mathrm{d}x \tag{1}$$

$$R_q = \sqrt{\frac{1}{L}\int_0^L [f(x)]^2\,\mathrm{d}x} \tag{2}$$

Fig. 1 [18] schematically shows various lengths used to characterize a surface profile (L_t=traverse length, L_e=evaluation length, L_s=sampling length, and L_c= cut-off length). The sampling length used to be called the cut-off length [18], and the number of sampling lengths (N_s) or the number of cut-off lengths (N_c) is typically five although it is three in Fig. 1.

Fig. 2 shows the roughness values of sample WC–Co-1 versus cut-off length L_c plotted on log–log scales. The value of R_q is always slightly larger than that of R_a under the same measuring conditions, and the trends for R_a and R_q are the same. Both R_a and R_q values increase with the increase of cut-off length.

When the cut-off length scale changes from 0.025 to 2.5 mm, the surface roughness R (R_a or R_q) and its difference ΔR depend on the cut-off length scale as a power law as shown below:

$$R \sim L_c^{\alpha} \tag{3}$$

$$\Delta R \sim (\Delta L_c)^{\alpha} \tag{4}$$

The exponent α has a special name, which is explained in the next paragraphs. The result shown in Fig. 2 conforms to the theory for self-affine fractal surfaces, which are explained in the next paragraphs, and therefore the ground surface of sample WC–Co-1 can be identified as a self-affine fractal surface.

Fractal objects that must be rescaled using an anisotropic transformation in order for the rescaled system to be identical with a part of the original system are called self-affine fractals. The scaling relation equation for a self-affine function can be [42]:

$$h(x) \sim b^{-\alpha} h(bx) \tag{5}$$

Where, $h(x)$ is a single-valued function, x is defined on the interval [0, 1], b is a constant, and α is called the Hölder or self-affine exponent and gives a quantitative measurement of the "roughness" of the function $h(x)$. An important result from Eq. (5) is related to the scaling of the height difference $\Delta h = |h(x_1) - h(x_2)|$ between two

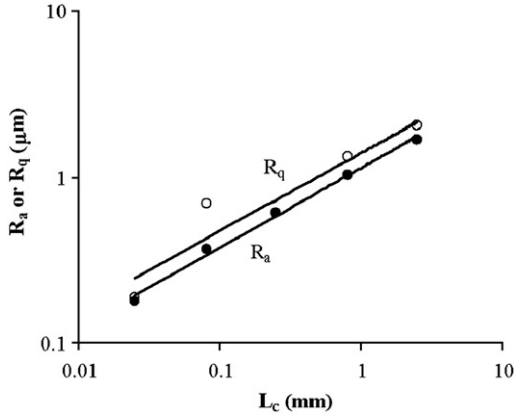

Fig. 5. Surface roughness R_a and R_q versus cut-off length L_c (sample WC–Co-2).

points separated by a distance $\Delta x = |x_1 - x_2|$. The solution of Eq. (5) is a power law [42]:

$$\Delta h \sim (\Delta x)^{\alpha} \tag{6}$$

Similarly, a self-affine fractal surface discussed in this section means a surface whose measured roughness depends on certain measuring length scale as a power law with a roughness exponent, α. The implications are discussed in Section 4. Reference [42] is recommended for more detailed explanations on self-affine fractals.

Fig. 3 shows the effects of number of sampling lengths N_s and sampling length L_s on R_a of sample WC–Co-1. Sampling length and number of sampling lengths also have effects on the R_a value.

The relationship between R_q and evaluation length L_e was also investigated [43]. Cut-off length L_c was fixed at 0.25 mm, and R_q was measured using various evaluation lengths. Fig. 4 shows surface roughness R_q versus evaluation length L_e plotted on log–log scales for the diamond ground WC–Co surface (sample WC–Co-1). When the evaluation length was changed from 0.25 mm to 2.5 mm, the roughness R_q was almost constant. The surface roughness of the ground WC–Co surface was found to be independent on the scale of evaluation length.

Fig. 5 shows the roughness values of sample WC–Co-2 versus cut-off length L_c plotted on log–log scales. Again, the value of R_q is always slightly larger than that of R_a under the same measuring conditions, and the trends for R_a and R_q are the same. Both R_a and R_q values increase with the increase of cut-off length. When the cut-off length scale changes from 0.025 mm to 2.5 mm, the surface roughness R (R_a or R_q) values depend on the cut-off length scale as a power law. The turned WC–Co surface can be also identified as a self-affine fractal.

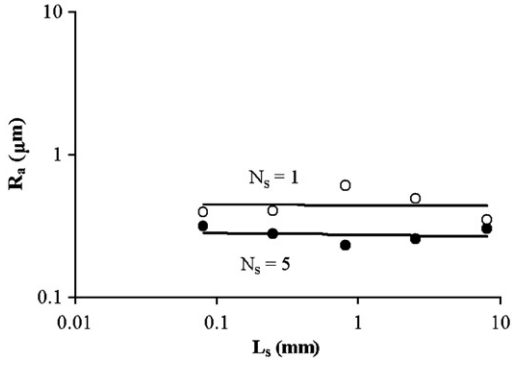

Fig. 6. Surface roughness R_a versus sampling length L_s with number of sampling lengths N_s = 1 and 5 (sample WC–Co-2).

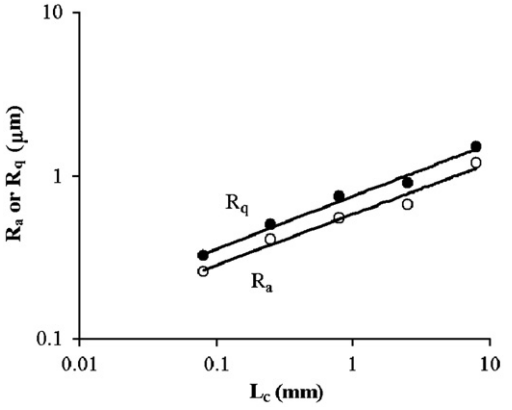

Fig. 7. Surface roughness R_a and R_q versus cut-off length L_c (sample Alloy-1, N_c = 1).

Fig. 6 illustrates the effects of sampling length L_s and number of sampling lengths N_s on R_a of sample WC–Co-2. Again, sampling length and number of sampling lengths have effects on the R_a value.

Fig. 7 shows the roughness values of the turned Alloy 625 coating (sample Alloy-1 Table 2) versus cut-off length L_c plotted on log–log scales. Both R_a and R_q values increase with the increase of cut-off length. When the cut-off length scale changes from 0.08 mm to 8 mm, the turned Alloy 625 surface of sample Alloy-1 can be identified as a self-affine fractal. Number of cut-off lengths has an influence on the R_a value but its effect is much smaller than that of cut-off length L_c as shown in Fig. 8 [44].

Let us consider the reasons for the results discussed above. A measured two-dimensional profile of a surface has different frequency components, and therefore a 'high-pass' filter with a cut-off length is used to cut low-

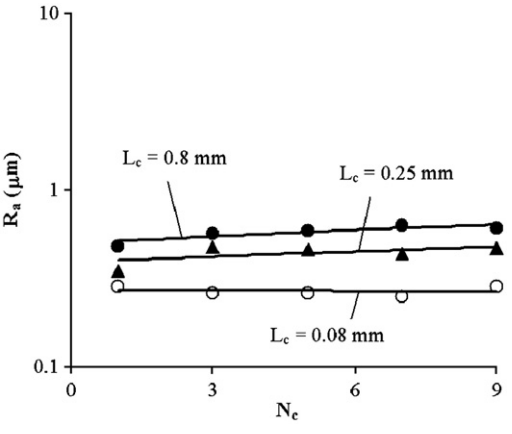

Fig. 8. Surface roughness R_a versus number of cut-off lengths N_c (sample Alloy-1).

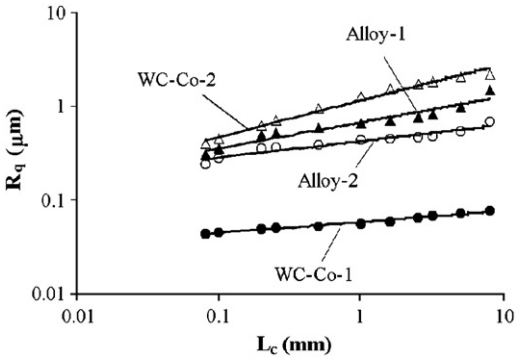

Fig. 9. Surface roughness R_q versus cut-off length L_c (four samples with different roughness exponents).

frequency data off to obtain a roughness profile and calculate the specified surface roughness height using the roughness profile. When a longer cut-off length was used, more data with lower-frequencies corresponding to waviness and even form irregularities could 'pass' the filter and therefore were included in the roughness profile. As a result, the calculated surface roughness value became larger.

Fig. 9 shows the differences of the roughness structures of the four sample surfaces with one factor: roughness exponent α [43]. For example, roughness exponents of samples Alloy-1 and Alloy-2 are 0.27 and 0.17 respectively. The difference of roughness exponents of these two samples is 0.1 on the cut-off scale from 0.08 mm to 8 mm. Using the roughness exponent is meaningful and straightforward to characterize the surface roughness of the precision-machined WC–Co and Alloy-625 coatings.

4. Discussion

Consider the meanings of the results shown in Fig. 9. WC–Co alloys are hard cutting-tool materials and are often used to machine various steels and alloys. To machine such hard WC–Co alloys, diamond turning and grinding operations can be performed. A mirror-like surface of the WC–Co coating sprayed on the steel rod by the HVOF process was obtained by fine grinding using the fine diamond wheel, and the surface finish of sample WC–Co-1 was the best in Fig. 9. Although diamond turning of WC–Co produced the worst surface finish on sample WC–Co-2 out of the four samples, it had a much higher MRR than the fine grinding as shown in Table 3. The machining time can be reduced, first by diamond turning to near the final dimensions and then by diamond grinding to obtain the required dimensions and surface finish.

WC–Co cutting tools are hard enough to machine Alloy 625, and can produce good surface finish on samples Alloy-1 and Alloy-2, better than that of turned WC–Co. As shown in Table 2, the machining conditions for samples Alloy-1 and Alloy-2 were the same except that the cutting tools were different. A special WC–Co (ISO M15) tool with coated TiAlN by physical vapor deposition, which had micro grains produced better surface finish on sample Alloy-2 than sample Alloy-1 that was turned using a typical WC–Co (ISO K20) tool.

Good surface finish can be reported by showing very low surface roughness heights measured using scanning probe microscopes such as AFMs. Most AFMs available in the market cannot scan a size larger than 0.1 mm. By scanning a very small area, very small surface roughness readings can be obtained, which however may not be suitable for comparison of surface quality with other published results obtained using stylus roughness testers, which use much longer cut-off lengths. Surface roughness values were found to increase following a power law of the cut-off length in this study and following a power law of the AFM scanning scale in our previous study [45]. Therefore, it would not be appropriate to directly compare any roughness heights obtained using different cut-off lengths or AFM scanning scales.

For a deterministic self-affine fractal, a system rescaled using an anisotropic transformation is identical with a part of the original system [42]. In this study, the precision-machined surfaces are characterized using Eqs. (1) and (2) by measuring R_a and R_q five times and taking the mean values as each roughness data. The obtained surface roughness depends on certain measuring length scale as a power law with a roughness exponent α, as shown in Fig. 9 and by Eqs. (3) and (4). Therefore, the precision-machined surfaces can be identified as self-affine fractals in a statistical sense within the correlation length, i.e. within the length scales studied from 0.08 to 8 mm.

The roughness exponent α is a useful parameter and can be used to predict a roughness value of the surfaces at any scale length within the correlation length [45]. This is because Eq. (4) can be used to calculate the roughness value at that scale length. It may be suitable to compare surfaces using roughness exponents, even if different cut-off lengths or scanning scales are used in the measurements.

5. Conclusion

Mirror-like surfaces were obtained by fine grinding using a fine diamond wheel for WC–Co coatings sprayed by the HVOF process. During the CBN

grinding of WC–Co coatings sprayed by the HVOF process, there were problems with loading of grinding wheels. This loading problem did not occur when diamond grinding was conducted. Surface roughness parameters R_a and R_q were measured using various cut-off lengths, sampling lengths, and numbers of sampling and cut-off lengths to characterize the scaling behavior of the surfaces. Precision-machined WC–Co and Alloy-625 surfaces could be identified as self-affine fractals in a statistical sense within the correlation length, i.e. within the length scales studied from 0.08 mm to 8 mm. The surface roughness heights of the machined surfaces were found to be dependent on the scale of cut-off length as a power law.

Acknowledgements

The first author wishes to express his appreciation for the measurement assistance provided by Ms. Sandy P.N. Yeong, Ms. N. Liu and Mr. Z.F. Peng of the School of MAE, Nanyang Technological University.

References

[1] Lansdown AR, Price AL. Materials to Resist Wear. Oxford: Pergamon Press; 1986. p. 96–8.
[2] Li CJ, Ohmori A, Harada Y. Formation of an amorphous phase in thermally sprayed WC–Co. J Therm Spray Technol 1996;5 (No 1):69–73.
[3] Okamoto S, Nakazono Y, Otsuka K, Shimoitani Y, Takada J. Mechanical properties of WC/Co cemented carbide with larger WC grain size. Mater Charact 2005;55(4–5):281–7.
[4] Prchlik L, Sampath S, Gutleber J, Bancke G, Ruff AW. Friction and wear properties of WC–Co and Mo–Mo_2C based functionally graded materials. Wear 2001;249(12):1103–15.
[5] Buytoz S, Ulutan M, Yildirim MM. Dry sliding wear behavior of TIG welding clad WC composite coatings. Appl Surf Sci 2005;252(5):1313–23.
[6] Li CJ, Ohmori A, Tani K. Effect of WC particle on the abrasive wear of thermally sprayed WC–Co coatings. Mater Manuf Process 1999;14(2):175–84.
[7] Asl SK, Sohi MH, Hokamoto K, Uemura M. Effect of heat treatment on wear behavior of HVOF thermally sprayed WC–Co coatings. Wear 2006;260(11−12):1203–8.
[8] Li CJ, Ohmori A, Harada Y. Effect of powder structure on the structure of thermally sprayed WC–Co coatings. J Mater Sci 1996;31:785–94.
[9] Yamane Y, Amano N, Hayashi K, Narutaki N. High speed machining of inconel 718 with ceramic tools. J Jpn Soc Precis Eng 1995;59(11):65–70.
[10] Zhong Z, Ramesh K, Yeo SH. Grinding of nickel-based superalloys and advanced ceramics. Mater Manuf Process 2001;16 (2):195–207.
[11] Cieslak MJ. The solidification behavior of an alloy 625/718 variant. Proceedings of the International Symposium on the Metallurgy and Applications of Superalloys 718, 625 and Various Derivatives, Pittsburgh, Pennsylvania; 1991. p. 71–80.
[12] Eiselstein HL, Tillack DJ. The invention and definition of alloy 625. Proceedings of the International Symposium on the Metallurgy and Applications of Superalloys 718, 625 and Various Derivatives, Pittsburgh, Pennsylvania; 1991. p. 1–14.
[13] Davidson JH. The influence of processing variables on the microstructure and properties of PM 625 alloy. Proceedings of the International Symposium on the Metallurgy and Applications of Superalloys 718, 625 and Various Derivatives, Pittsburgh, Pennsylvania; 1991. p. 229–39.
[14] Vernot-Loier C, Cortial F. Influence of heat treatments on microstructure, mechanical properties and corrosion behaviour of alloy 625 forged rod. Proceedings of the International Symposium on the Metallurgy and Applications of Superalloys 718, 625 and Various Derivatives, Pittsburgh, Pennsylvania; 1991. p. 409–22.
[15] Wilson ILW, Gourley RG, Walkosak RM, Bruck GJ. The effect of heat input on microstructure and cracking in alloy 625 weld overlays. Proceedings of the International Symposium on the Metallurgy and Applications of Superalloys 718, 625 and Various Derivatives, Pittsburgh, Pennsylvania; 1991. p. 735–47.
[16] Capitanescu D. Alloy 625 weld overlays for offshore and onshore projects. Proceedings of the International Symposium on the Metallurgy and Applications of Superalloys 718, 625 and Various Derivatives, Pittsburgh, Pennsylvania; 1991. p. 821–35.
[17] Moran AL, Palko WA, Madden CJ, Kelley P. Spray formed alloy 625 tubulars. Proceedings of the International Symposium on the Metallurgy and Applications of Superalloys 718, 625 and Various Derivatives, Pittsburgh, Pennsylvania; 1991. p. 843–9.
[18] Whitehouse DJ. Handbook of Surface Metrology. Bristol, UK: Institute of Physics Publishing; 1994. p. 6–716.
[19] Morehead M, Huang Y, Hartwig KT. Machinability of ultrafine-grained copper using tungsten carbide and polycrystalline diamond tools. Int J Mac Tools Manuf 2007;47(2):286–93.
[20] Yin L, Pickering JP, Ramesh K, Huang H, Spowage AC, Vancoille EYJ. Planar nanogrinding of a fine grained WC–Co composite for an optical surface finish. Int J Adv Manuf Technol 2005;26(7–8):766–73.
[21] Shi XL, Shao GQ, Duan XL, Xiong Z, Yang H. Characterizations of WC−10Co nanocomposite powders and subsequently sinterhip sintered cemented carbide. Mater Charact 2006;57(4–5):358–70.
[22] Wilson GF, Alworth R, Ramalingam S. Machining sintered carbides with polycrystalline diamond tools, machining hard materials. In: Williams R, editor. Dearborn: Society of Manufacturing Engineers; 1982. p. 104–9.
[23] Poulopoulos P, Lindner J, Farle M, Baberschke K. Changes of magnetic anisotropy due to roughness: a quantitative scanning tunneling microscopy study on Ni/Cu(001). Surf Sci 1999;437 (3):277–84.
[24] Chawla N, Holmes JW, Mansfield JF. Surface roughness characterization of Nicalon™ and HI-Nicalon™ ceramic fibers by atomic force microscopy. Mater Charact 1995;35(4): 199–206.
[25] Basavarajappa S, Chandramohan G, Rao KVN, Radhakrishanan R, Krishnaraj V. Turning of particulate metal matrix composites — review and discussion. Proc Inst Mech Eng B J Eng Manuf 2006;220(7):1189–204.
[26] Zhong ZW, Lu YG. 3D characterization of super-smooth surfaces of diamond turned OFHC copper mirrors. Mater Manuf Process 2002;17(2):269–80.
[27] Zhong Z, Lee WY. Grinding of silicon and glass using a new dressing device and an improved coolant system. Mater Manuf Process 2001;16(4):471–82.

[28] Zhong ZW, Tok WH. Grinding of single-crystal silicon along crystallographic directions. Mater Manuf Process 2003;18 (5):811–24.
[29] Young HT, Liao HT, Huang HY. Surface integrity of silicon wafers in ultra precision machining. Int J Adv Manuf Technol 2006;29(3–4):372–8.
[30] Zhong Z. New grinding methods for aspheric mirrors with large curvature radii. Ann CIRP 1992;41(1):335–8.
[31] Zhong Z, Nakagawa T. Grinding of aspherical SiC mirrors. J Mater Process Technol 1996;56(1−4):37–44.
[32] Mainsah E, Greenwood JA, Chetwynd DG. Metrology and Properties of Engineering Surfaces. Boston: Kluwer Academic Publishers; 2001. p. 1–32.
[33] Tsai MJ, Huang JF. Efficient automatic polishing process with a new compliant abrasive tool. Int J Adv Manuf Technol 2006;30 (9–10):817–27.
[34] Meneghello R, Concheri G, Savio G, Comelli D. Surface and geometry error modeling in brittle mode grinding of ophthalmic lenses moulds. Int J Mach Tools Manuf 2006;46(12–13):1662–70.
[35] Zhong ZW, Jiang Y. LED lighting configurations for visual inspection of IC packages. Mater Manuf Process 2004;19 (3):439–49.
[36] Griffiths B. Manufacturing Surface Technology. London: Penton Press; 2001. p. 70–115.
[37] Hayden BE. Surface Science. New York: Adam Hilger; 1992. p. S1–9.
[38] Stout KJ, Blunt L. Three-dimensional surface topography. London: Penton Press; 1994. p. 82–102.
[39] Lu YG, Zhong ZW, Yu J, Xie HM, Ngoi BKA, Chai JB, et al. Thermal deformation measurement of electronic packages using atomic force microscope scanning moiré technique. Rev Sci Instrum 2001;72(4):2180–5.
[40] Dynamic Ceramic, Hardness, http://www.dynacer.com/hardness.htm, visited on 26 March 2007.
[41] Process Technology Division. Technical Report. Singapore: Gintic Institute of Manufacturing Technology; 1997. p. 15–25.
[42] Barabasi AL, Stanley HE. Fractal Concepts in Surface Growth. Cambridge: Cambridge University Press; 1995. p. 32–6.
[43] Z.F. Peng, Study of Fractal Roughness Structure of Precision Machined Surfaces, MSc Dissertation of Nanyang Technological University, Singapore, 2005, pp. 52–55 and pp. 68–69.
[44] N. Liu, Analysis of Precision Machined Surfaces, MSc Dissertation of Nanyang Technological University, Singapore, 2005, pp. 60–62.
[45] Zhong ZW, Lu YG. Fractal roughness structure of diamond-turned copper mirrors. Mater Manuf Process 2003;18(2):219–27.